HHS Public Access

Author manuscript

Free Radic Biol Med. Author manuscript; available in PMC 2021 December 13.

Published in final edited form as:

Free Radic Biol Med. 2021 June ; 169: 416–424. doi:10.1016/j.freeradbiomed.2021.04.030.

Iron-binding cellular profile of transferrin using label-free Raman hyperspectral imaging and singular value decomposition (SVD)

Kate Tubbesing[a,1], **Ting Chean Khoo**[a,1], **Shahab Bahreini Jangjoo**[a], **Anna Sharikova**[a], **Margarida Barroso**[b], **Alexander Khmaladze**[a,*]

[a]Physics Department, SUNY University at Albany, 1400 Washington Avenue, Albany, NY, 12222, USA

[b]Department of Molecular and Cellular Physiology, Albany Medical College, 47 New Scotland Avenue, Albany, NY, 12208, USA

Abstract

Serum transferrin (Tf) is the essential iron transport protein in the body. Transferrin is responsible for the sequestration of free iron in serum and the delivery of iron throughout the body and into cells, where iron is released inside a mildly acidified endosome. Altered iron distributions are associated with diseases such as iron-overload, cancer, and cardiovascular disease. The presence of free iron is linked to deleterious redox reactions, inside and outside cells and organelles. As Tf iron release is pH dependent, any changes in intraorganelle and extracellular pH, often associated with disease progression, could inhibit normal iron delivery or accelerate iron release in the wrong compartment. However, imaging approaches to monitor changes in the iron-bound state of Tf are lacking. Recently, Raman spectroscopy has been shown to measure iron-bound forms of Tf in solution, intact cells and tissue samples. Here, a biochemical Raman assay has been developed to identify iron-release from Tf following modification of chemical environment. Quantitative singular value decomposition (SVD) method has been applied to discriminate between iron-bound Tf samples during endocytic trafficking in intact cancer cells subjected to Raman hyperspectral confocal imaging. We demonstrate the strength of the SVD method to monitor pH-induced Tf iron-release using Raman hyperspectral imaging, providing the redox biology field with a novel tool that facilitates subcellular investigation of the iron-binding profile of transferrin in various disease models.

Keywords

Transferrin; Iron; Redox biology; Cancer; Raman hyperspectral imaging

*Corresponding author. akhmaladze@albany.edu (A. Khmaladze).
[1]co-first authors.

Declaration of competing interest

The authors declare no competing interests.

Appendix A. Supplementary data

Supplementary data to this article can be found online at https://doi.org/10.1016/j.freeradbiomed.2021.04.030.

1. Introduction

One of the most important biological functions of transferrin (Tf) in serum is iron sequestration, which prevents lipid peroxidation and unregulated redox reactions [1]. In the neutral pH of serum (~7.4), iron-free transferrin (apo-Tf) binds two ferric iron molecules to become holo-Tf [2], which can then bind the transferrin receptor (TfR) at the cell surface. The TfR-Tf complex undergoes clathrin mediated endocytosis to deliver iron into the cells. Inside mildly acidified early endosomes, iron is released from Tf for utilization or storage [2]. Importantly, apo-Tf is recycled to the cell surface where Tf is released from TfR to undergo iron-binding in the neutral pH of serum and repeat the cycle [1]. There are many steps in this process where regulation of pH could be disrupted either inside endosomes or in the extracellular domain of diseased tissue [3–6]. Thus, altered pH regulation could disrupt iron transport, which is essential to human health [1].

As Tf iron-release occurs upon pH acidification, it is proposed that methods of monitoring Tf iron release may provide insights into the complex regulation of pH and iron transport in cells and tissues. A method to investigate Tf iron release requires a label-free, non-invasive and non-destructive method, such as Raman hyperspectral imaging, that can discriminate between holo- and apo-Tf forms in intact cells [7]. Importantly, this technique allows for mapping of the iron-bound Tf populations overlaid on the brightfield image of the intact cells. A unique control for these experiments includes oxalate modified Tf (oxa-Tf), which does not efficiently release iron in a mildly acidified endosome [8], and is used as a marker of iron-bound Tf profile. Here, we expand our understanding of Raman imaging of the Tf iron-binding profile with evaluation of several processing methods for both biochemical analysis of purified Tf and Raman hyperspectral imaging of intact cells.

Vibrational spectroscopic methods, including Raman microscopy, can be used to identify unique chemical signatures of complex biological samples via inelastic scattering [7,9–17]. Raman scattering occurs when the energy exchanged between an incident photon and a molecule leads to a shift in the wavelength of light that can be detected following Rayleigh filtration. These scattered photons provide information about the chemical structure of the sample. Raman microspectroscopy can be performed on a homogeneous solution, as well as in more complex samples, using a modified laser-scanning confocal system. Raman hyperspectral imaging provides correlation of unique Raman signatures to specific pixels, and thus a spatial assignment of Raman peaks at subcellular level can be achieved. Recently, we identified Raman peak at 1300 cm^{-1} as a useful marker for monitoring the relative levels and location of iron-bound Tf within complex cell and tissue samples [7]. To further explore this method, we conducted more extensive biochemical studies with purified Tf proteins, including a biochemical assay to evaluate Tf iron-release. Additionally, an alternative post-processing approach with multivariate analysis was used to evaluate potential changes in the Tf iron binding profile, occurring in cells following Tf internalization over time. The multivariate approach is beneficial, as it avoids the reliance on a single peak and provides a robust approach for future investigations of iron binding properties of transferrin in cells and tissues.

Multivariate analysis methods, including principal component analysis (PCA) and singular value decomposition (SVD), can be used to analyze complex Raman data [18–21]. Both methods, known as dimension reduction techniques, are applied to reduce the high dimensionality data into lower dimensionality data. PCA method generates the eigenvectors and eigenvalues from the covariance matrix, while SVD method decomposes the input matrix into three separate matrices that contain the eigenvectors and eigenvalues [22]. Here, we demonstrate that SVD is a robust and reliable post-processing method to discriminate between different Raman hyperspectral datasets. The SVD methodology allows us to automatically differentiate entire Raman spectra and easily obtain crucial information about the differences between the spectra collected from different intact cells or regions within the cells.

Therefore, to clarify, the SVD analysis facilitates the co-distribution, or clustering, of spectral data by automatically finding similarities in Raman peak position, width and intensity within the spectra of the entire dataset, while the spectra with different spectral features will be placed farther apart on the SVD scatter plot. Each point on the SVD plot represents a single Raman spectrum. The SVD components shown in the accompanying graphs allow the identification of significant spectral regions (reported as Raman Shift, cm^{-1}) that contribute to the scatter plot distributions. The incorporation of SVD into the Raman data analysis helps to extract important information about the heterogeneity of samples, and the effects of various conditions on cells, previously hidden in the large amount of spectral data [9,23]. Importantly, the use of SVD can reduce our dependence on specific peaks when evaluating complex samples. Raman-based quantification of Tf iron-release in purified Tf protein and in endocytic iron-release cellular studies provides a unique and novel approach to study this important biological process in vitro and in vivo, respectively.

2. Experimental (materials and methods)

2.1. Transferrin preparation, validation, and iron-release assay

Apo-Tf, holo-Tf and oxa-Tf were prepared and validated as published [7]. Purified protein was imaged in neutral phosphate buffered saline (PBS) or subjected to an iron-release assay in the presence of 200 mM MES buffer, 300 mM KCl, pH 5.5 with 8 mM EDTA to stimulate iron release [24]. Control conditions for iron-release assay included the addition of PBS at the equivalent volume of utilized MES buffer (final volume increased by 1/3); this control condition accounted for any decrease in peak intensities associated with decreased protein concentration.

2.2. Cell culture and transferrin internalization assay

T47D cells were obtained from ATCC and cultured in DMEM with 10% fetal bovine serum, and 4 mM L-glutamine, pH 7.4. Experiments were performed using cells passaged less than 20 times; cells were plated onto quartz substrates coated in poly-D-lysine and incubated 24–36 h. Prior to Tf internalization, cells were pre-incubated with clear imaging media (phenol-free DMEM 0.5% bovine serum albumin, 4 mM L-gluta-mine, pH 7.4) for 30 min. Then they were incubated with Tf forms (apo, holo or oxa) at a concentration of 50 μg/mL for 5 min at 37 °C. Following initial incubation, cells were either washed and fixed (5 min

time point) or washed and chased for additional 55 min before fixation (60 min time point). Control cells were not incubated with Tf, but underwent the same treatment process with clear imaging media alone. Fixation was performed using ice cold 4% paraformaldehyde for 15 min. Cells were stored and imaged in PBS. To ensure that no unintended pH-induced Tf conformation changes have occurred, all media, buffers, and fixation solutions where freshly prepared and maintained at a neutral pH. The contrast between the changes in oxa-Tf and holo-Tf Raman signatures, from early endocytic to late endocytic steps, is an internal control mechanism to ensure the pH sensitive iron-binding behavior of the unlabeled protein is as expected.

2.3. Raman microscopy and analysis

Raman spectra were collected by HORIBA XploRA PLUS Raman microscope. The system was equipped with a 1024 × 256 TE air cooled CCD chip (pixel size 26-μm, temperature −60 °C). Entrance slit was set to 50 μm, which resulted in spectral resolution of 4 cm^{-1}. The protein solutions and cells were imaged with a 20 × immersion objective (Olympus UMPlanFLN 20 ×, N/A 0.5); excitation laser wavelength was 532 nm. Accumulation, collection time and laser power were kept constant for any data set collected. Protein samples were subjected to point-scan measurements, while data on intact cells was collected by hyperspectral imaging of regions of interest (ROIs). Each individual pixel had an associated Raman spectrum, which was an average of three sequentially collected spectra (accumulation feature), subjected to automatic LabSpec de-spiking filter. HORIBA LabSpec6 software was used for noise reduction, normalization, and fluorescent background removal prior to further analysis. Single-peak quantification and the peak intensity-based hyperspectral overlay are performed as previously described [7].

2.4. SVD analysis of Raman datasets

All spectra from each imaging set were grouped together and formed an input matrix for the SVD algorithm, which was implemented as an in-house LabVIEW program. Raman spectra from each point in the imaging set were grouped together to form a matrix X, with matrix size (m × n), where m is the number of points in a spectrum (m = 400), and n is the number of spectra in a set (n = 1200 combining 300 spectra for apo-, holo-, oxa-Tf and control). The SVD algorithm was applied to the matrix X to separate it into matrices U, ∑ and V using Matlab SVD function. Individual columns extracted from the matrix V, such as V1 and V2, representing the projection of each spectrum on the corresponding SVD component Ui, were plotted as the SVD scatter plot, while the corresponding SVD components (essentially, the eigenvectors of the decomposition) extracted from the matrix U, such as U1 and U2, were plotted in the accompanying graph. The color of every 300 point group on the SVD scatter plot was changed to distinguish the spectra of apo-, holo-, oxa-Tf and control. Manually applied dotted line shows the separation between the iron bound and iron free region. Addition information on SVD analysis is provided in Supplementary Methods.

3. Results

3.1. SVD analysis provides a method of distinguishing apo-Tf, holo-Tf, and oxa-Tf purified proteins in solution

The Raman spectra of different iron-binding forms of Tf protein solutions at a concentration of 5 mg/mL in PBS were collected and analyzed using SVD methodology. Apo-Tf and holo-Tf are the iron-free and iron-bound Tf forms, respectively, whereas oxa-Tf is a chemically modified form of iron-bound Tf, which releases iron at a significantly slower rate than holo-Tf in an acidified environment [8]. Raman spectra of all protein solutions had a visible phenylalanine peak and prominent peaks associated with iron-loaded Tf samples, including 1170 cm^{-1}, 1277 cm^{-1}, 1500 cm^{-1} and 1600 cm^{-1} [7,25]. As shown in Fig. 1A, apo-Tf, holo-Tf and oxa-Tf were well separated within the SVD scatter plot. Importantly, the leading component of the SVD analysis that discriminates apo-Tf, holo-Tf and oxa-Tf into separate clusters shows high intensity at the iron-associated peaks, e.g. 1170 cm^{-1}, 1277 cm^{-1}, 1500 cm^{-1} and 1600 cm^{-1} (Fig. 1B). It should be noted that peaks associated with leading components are not always obvious in the examination of individual spectra, for example, the 1600 cm^{-1} peak is often incorporated into a larger amine associated peak at ~1520–1720 cm^{-1} (Supplementary Fig. 1). Thus, the separation between the apo-Tf, holo-Tf and oxa-Tf Raman spectra is primarily influenced by the iron-binding state of the protein, as 1170 cm^{-1}, 1277 cm^{-1}, 1500 cm^{-1} and 1600 cm^{-1} peaks have previously been associated with the iron-bound form of Tf specifically [7,26]. Interestingly, the two iron-binding Tf proteins, holo-Tf and oxa-Tf, can be effectively separated by SVD analysis (Fig. 1A), indicating that SVD can detect structural differences between holo-Tf and oxa-Tf, such as the replacement of carbonate for an oxalate at the synergistic anion iron-binding motifs [8]. Therefore, we cannot dismiss the role of oxalate itself contributing to the SVD separation. Pure oxalate Raman spectra suggest its contribution to shifts near 1500 cm^{-1} (https://spectrabase.com/spectrum/4aZtRqc8ite). Similar separation of Tf forms was observed in the SVD analysis of Raman spectra of the dehydrated Tf samples (Supplementary Fig. 2). In summary, the leading component peaks underlying the separation between apo-Tf and iron-binding Tf forms are associated with holo-Tf [7,25], while oxalate coupling at the anion iron-binding motif appears to be enough to separate holo-Tf from oxa-Tf using Raman spectra of Tf purified proteins in solution.

3.2. Iron-release from purified Tf in solution is accompanied by reduction in 1277 cm^{-1} Raman peak intensity

Transferrin has evolved to release iron inside a mildly acidic endosome while attached to its receptor, and this process of Tf iron-release has been studied in detail using purified samples in solution [24]. However, it remains unclear how the changes in the extracellular environment influence the iron-bound state of soluble Tf. Here, we demonstrate a reproducible and quantifiable reduction in the 1277 cm^{-1} Raman peak when purified holo-Tf protein undergoes pH-mediated iron-release in solution.

Raman spectra were collected from the Tf samples before and after treatment with either a neutral PBS buffer or an acidified iron-release MES buffer [24]. Representative control spectra of holo-Tf proteins in solution before and after the addition of neutral PBS buffer

demonstrate that a 1/3 dilution will not significantly reduce the 1277 cm^{-1} Raman peak. The dilution with PBS slightly reduces the overall intensity of the Raman spectrum, without any other pronounced changes (Fig. 2A–B). Representative spectra of holo-Tf before and after treatment with an acidic MES buffer show the reduction of not only the 1277 cm^{-1} peak, but also the other peaks associated with iron-bound Tf, including 1500 cm^{-1} and 1600 cm^{-1} (Fig. 2C). However, a statistically significant, reproducible drop in the 1277 cm^{-1} peak intensity following the addition of iron-release buffer alone is sufficient to monitor iron release (Fig. 2D). The reproducibility of the reduction in iron-bound Tf peak at 1277 cm^{-1} upon the addition of iron-release buffer is demonstrated in Supplementary Fig. 3. Moreover, a multivariate SVD analysis was used to separate the iron-bound Tf from iron-released form in this assay (Fig. 2E). Upon the evaluation of leading components (Fig. 2F), which included iron-associated 1277 cm^{-1} and 1600 cm^{-1} peaks, a large contribution at 1040 cm^{-1}, which is associated with the MES buffer (https://spectrabase.com/spectrum/17wMBi0gP1U), has also been observed. This contribution of the MES buffer to the Raman spectra is a visible as peak ~1040 cm^{-1} in the representative spectra (Fig. 2C). Notably, when the SVD analysis excluded the spectral region below 1100 cm^{-1}, which was associated with MES buffer (Fig. 2G–H), the iron-bound Tf remained well separated from the iron-released Tf form (Fig. 2G). Further, through the exclusion of spectral region below 1100 cm^{-1} in the SVD analysis, the peak at 1277 cm^{-1}, associated with iron-bound Tf, becomes a leading component contributing to SVD separation (Fig. 2H).

3.3. Raman hyperspectral imaging and SVD analysis of breast cancer cells incubated with apo-Tf, holo-Tf, or oxa-Tf

Cellular Tf-TfR complexes are transported via a mildly acidified endosome to release iron, and then continue through the endocytic recycling pathway before returning to the surface, where Tf is released to repeat the cycle [2]. The time for one Tf-TfR transport cycle can vary depending on cell type; however, in general, the longer the Tf-TfR complexes take to travel through the cell, the more likely they will have time to release iron for cellular utilization. Previously, we have demonstrated that the 1277 cm^{-1} peak in purified Tf protein shifts closer to 1300 cm^{-1} when iron-bound Tf is measured in cells and tissues [7].

Here, we further evaluated Raman microscopy datasets using SVD analysis on human breast cancer T47D cells, which display high TfR expression [27,28]. T47D cells were incubated with unlabeled apo-Tf, holo-Tf, or oxa-Tf for 5 min, and either followed, or not, by an additional 55 min chase to allow for complete iron-release from holo-Tf. Negative control cells were subjected to similar protocol in the absence of added Tf. Cells were fixed and subjected to Raman hyperspectral imaging with subsequent fluorescent background subtraction and normalization to the phenylalanine peak at ~1003 cm^{-1} for peak quantification and hyperspectral mask creation. An important distinction between the evaluation of the 1300 cm^{-1} peak for quantification and the SVD analysis is how the negative control cells are utilized. In quantification of 1300 cm^{-1} peak, the negative control cells are used to determine the average background contribution of the 1300 cm^{-1} region, which is subtracted from the apo-Tf, holo-Tf and oxa-Tf data sets. In the SVD analysis, the negative control cell data can be incorporated into the analysis and are predicted to behave similarly to apo-Tf at the 5 min time point.

Most of holo-Tf, and even more so for oxa-Tf, should be in the iron-bound state at the 5 min time-point. Apo-Tf, although iron-free when added to cells, can still bind iron from the media for delivery into cells; however, this event is not frequent under our experimental conditions [7]. Representative spectra for 5 min incubation with apo-Tf, holo-Tf and oxa-Tf are shown in Fig. 3A, with the iron-bound Tf peak at 1300 cm^{-1} highlighted. Negative control untreated cells were utilized for the calculation of the background threshold when the 1300 cm^{-1} peak was quantified, as described above. The distribution of the 1300 cm^{-1} peak intensity within cells is converted to an intensity-based hyperspectral map, which is superimposed on the cell images in Fig. 3B. The hyperspectral image provides visualization of the dispersed, high intensity Tf-associated pixels in the cells incubated with holo-Tf or oxa-Tf for 5 min. Quantification of the 1300 cm^{-1} peak shows that apo-Tf is significantly lower in intensity than either holo-Tf or oxo-Tf, as expected (Fig. 3C). The SVD analysis of Raman spectra shows that following 5 min incubation, cells with holo-Tf and oxa-Tf are grouped together, while apo-Tf is more separated and overlaps with negative control cells (Fig. 3D). There is some overlap between the four groups at this time point, which is to be expected, as not all pixels may represent cell regions with Tf-filled endocytic vesicles, and each pixel may include apo-Tf as well as holo-Tf or oxa-Tf. The apo-Tf is a flawed negative control, since it can bind extracellular iron at a neutral pH and undergo TfR mediated endocytosis, although at much lower frequency than cells incubated with iron-loaded holo-Tf. The evaluation of the dominant SVD components separating these populations has identified a significant contribution of the iron-bound Tf peak at 1300 cm^{-1} (Fig. 3E). Other significant features include regions around 1434–44 cm^{-1} and 1660–70 cm^{-1}, which are associated with a CH_2 deformation of lipids and amide I, respectively [29].

At the 60 min time-point, in the experiment where cells are incubated with Tf for 5 min and then chased with media for an additional 55 min, it is expected that holo-Tf will have completely released all its associated iron, unlike oxa-Tf, which should retain a significant amount of iron even after 60 min. The holo-Tf, apo-Tf and negative control cell samples are expected to behave similarly, as any minor iron-binding to apo-Tf should not significantly impact the cells at this point. Representative spectra for 60 min incubation with apo-Tf, holo-Tf and oxa-Tf are shown in Fig. 4A, with the iron-bound Tf peak at 1300 cm^{-1} highlighted. A panel of representative hyperspectral maps for each condition shows that at the 60 min time-point, only oxa-Tf displays high intensity regions associated with the iron-bound Tf peak at 1300 cm^{-1} (Fig. 4B). Quantification of the 1300 cm^{-1} peak shows that oxa-Tf is significantly higher in intensity levels than either apo-Tf or holo-Tf (Fig. 4C). The SVD analysis of Raman spectra for this time point demonstrates that the apo-Tf, holo-Tf and negative control significantly overlap, and are completely separated from the oxa-Tf population (Fig. 4D). The leading SVD components at 60 min (Fig. 4E) are not that different from those in the 5 min data-point experiment (Fig. 3E). They include iron-bound Tf peak at ~1300 cm^{-1}, in addition to the lipid and amide peaks at 1434 cm^{-1} and 1650 cm^{-1} respectively (Fig. 4E). The SVD component peak at ~1050 cm^{-1} is likely directly associated with a Raman shift as a result of oxa-Tf in cells, with similar peaks in ~1050 cm^{-1} region being previously associated with C–O stretching of proteins [29].

The SVD scatter plots from three independent experiments were subjected to the analysis of population distributions, to evaluate how Tf populations shift between early endocytic

time points (5 min, Fig. 3D, Supplementary Fig. 6) and later time points (60 min, Fig. 4D, Supplementary Fig. 7). The placement of the dotted line was based on the oxa-Tf population, and it was expected that spectra of cell regions with iron-bound Tf would fall into the same region of the SVD scatter plot as oxa-Tf (iron-bound, positive control). In Fig. 5A, following 5 min Tf incubation, there is a small amount of the apo-Tf and larger population of holo-Tf segregated to the iron-bound Tf region of the scatter plot, in the same region as oxa-Tf. However, in Fig. 5B at the late endocytic time point, a population shift occurs, and oxa-Tf is completely separated from negative control cells and those incubated with apo-Tf or holo-Tf. It should be noted that here the oxa-Tf is a positive control, the basis of the iron-bound Tf region and line placement that facilitates this quantitative approach. This suggests that SVD analysis of Raman hyperspectral cell data can be used to demonstrate the unloading of iron from wildtype Tf via analysis of early and late endocytic time points.

In summary, the Raman hyperspectral imaging can be applied to distinguish forms of iron-bound Tf in-vitro and in complex cellular environments using either the analysis of specific peaks or through the multivariate SVD analysis. The decision to select one or both methods to evaluate the Raman microscopy spectral data should be determined by the specific experimental design. In-vitro methods, which facilitate identification of Tf iron-release upon modification of chemical environment of Tf sample, are robust and reproducible. Here the SVD analysis provided insights into the iron-dependent changes in complex Raman cellular signatures, revealing distinct iron binding profiles of transferrin during endocytic uptake in breast cancer cells.

4. Discussion

Raman spectroscopy as a non-invasive, non-destructive imaging method has been widely applied in the analysis of biochemical materials both in research and clinical settings [13,29–35]. Previously, we have demonstrated the importance of 1300 cm^{-1} peak in identification of iron-bound Tf in cells and tissues, and focused on the endocytic patterns of breast cancer cells with known disrupted endocytic trafficking [7,36]. Here, we have focused on the incorporation of SVD analysis into the study of purified Tf proteins in solution and into the cell-based Tf uptake assays. The SVD analysis is crucial to highlight multiple but often rather small changes in the Raman spectra, particularly when dealing with the analysis of complex cellular samples (Figs. 3–5). Moreover, SVD analysis provides information about the leading SVD components, which represent significant changes in the spectral regions that separate the samples, and would have been lost if the Raman spectra were merely averaged for comparison. It is important to not only perform the SVD analysis on Raman spectra of biological samples, but also dissect the SVD components for biological significance, as discussed below.

Raman spectra of purified transferrin can vary based on protein concentration, iron content, glycosylated form, laser wavelength and instrumental sensitivity [25,26,37]. However, there have been several Raman spectral regions consistently associated with iron-bound Tf, which were also identified in the leading components in the SVD analysis of purified Tf samples, including 1170 cm^{-1}, 1277 cm^{-1}, 1500 cm^{-1} and 1600 cm^{-1} (Fig. 1B). Upon subjecting

purified holo-Tf samples to an iron-release solution assay, the Raman peak at 1277 cm^{-1} proved to be an ideal indicator of the presence of iron-bound Tf, as it was significantly reduced upon the addition of the acidic iron-releasing buffer (Fig. 2D). We subjected the same data set to two separate SVD analyses, which varied in the Raman spectral range, to address Raman signatures assigned to iron-release solutions (Fig. 2E–H). We showed that the change in buffer solutions can be controlled for in analysis by restricting the spectral regions in SVD processing. In general, this indicates that using both the single peak quantification and multivariate analysis is beneficial for robust Tf iron-release studies involving modifications to the chemical environment of the purified Tf. Raman analysis of the iron-release solution assay is a promising method with potential uses for biologists studying how changes to the extracellular environment may influence Tf iron-release.

Previously, we have shown that the dominant iron-bound Tf peak in the 1277 cm^{-1} region shifted toward ~1300 cm^{-1} in cells [7], and this peak was used to identify iron-bound Tf with Raman hyperspectral imaging (Fig. 3B–C). Other cellular components, such as fatty acids, may contribute to the region around ~1300 cm^{-1} [29]. To ensure we only picked up the iron-bound Tf signal, a negative control (T47D cells without added unlabeled Tf proteins) were used to generate a background value, which was then subtracted from the intensity measurements of cells incubated with Tf [7]. Thus, the quantification of the 1300 cm^{-1} peak intensities in the iron-release solution assay at 5 min could be used to distinguish cells that had significant amounts of internalized iron-bound Tf (holo-Tf and oxa-Tf, Fig. 3C). In addition, upon providing the additional time for the holo-Tf to release iron inside the cells, at 60 min timepoint the oxa-Tf samples were the only ones with high 1300 cm^{-1} peak intensities, just as expected (Fig. 4C). While the quantification based on the 1300 cm^{-1} peak alone was reliable, the evaluation of the same population with the SVD analysis did not require the subtraction of the average intensity of negative control cells at 1300 cm^{-1}.

The SVD analysis proved to be a reasonably robust method for separating the iron-bound Tf containing cells (holo-Tf and oxa-Tf) at early incubation times (5 min) from the cells that were not exposed to iron-bound Tf (Figs. 3D and 5A). At a later (60 min) time point, the oxa-Tf stands completely apart from apo-Tf, holo-Tf and control cells in the SVD plot, indicating that its Raman spectra by then are substantially different. The overlap of the apo-Tf, holo-Tf and control cells in this plot is a clear indication that holo-Tf has released its iron by 60 min post internalization (Figs. 4D and 5B). The leading SVD components of both the 5 min and 60 min time points included, apart from the peak at ~1300 cm^{-1}, noticeable contributions at 1434 cm^{-1} and 1650 cm^{-1} (Figs. 3E and 4E). Since the peak at 1650–70 cm^{-1} is associated with amide I [29], it is reasonable to assume that the addition of Tf protein, independently of iron state, influenced the protein conformation, and therefore the Raman spectra. As the 1434 cm^{-1} peak has been associated with CH_2 deformation, lipids and acyl groups [29], it is difficult to assign a specific biological change that is occurring. Considering that the addition of holo-Tf was specifically associated with alterations in the rates of clathrin-mediated endocytosis [38], there could also be changes in lipid composition responsible for the presence of 1434 cm^{-1} peak in the SVD component.

5. Conclusion

Raman microscopy is well suited for the evaluation of extracellular and intracellular factors influencing Tf iron-release. Importantly, these methods do not require any labeling of the specimens. This work provides a reliable and robust methodology to monitoring iron release both in purified Tf protein solutions and in intact cells subjected to endocytic trafficking studies. Here, we show that methods for evaluating Tf iron-binding properties in complex biological samples should ideally include both individual Raman peak quantification and the SVD analysis. The 1300 cm^{-1} Raman peak alone can be used for identification of iron-bound Tf populations using hyperspectral visualization overlays in cells and tissue. The SVD analysis provides a robust, unbiased method of evaluating multiple changes in the Raman spectra that can be easily overlooked when complex cell spectra are evaluated. In summary, Raman micro-spectroscopy combined with SVD analysis is an excellent tool that can further elucidate the downstream effects of Tf mediated iron delivery in a broad range of specimens and conditions.

Supplementary Material

Refer to Web version on PubMed Central for supplementary material.

Funding

This work was supported by the National Institutes of Health RO1 CA207725 and RO1 CA233188 to Dr. Barroso and RO1 DA047410-01 grant to Dr. Khmaladze.

Availability of data and material

Data sets are available upon request through the corresponding author.

Abbreviations:

Apo-Tf	Transferrin protein without bound iron, has ability to bind available iron at neutral pH
EDTA	Ethylenediaminetetraacetic acid (common biological chelator)
HEPES	4-(2-hydroxyethyl)-1-piperazineethanesulfonic acid (common biological buffer)
Holo-Tf	Transferrin protein with iron in both lobes, can release iron in acidic environment
MES	2-(*N*-morpholino) ethanesulfonic acid (common biological buffer)
Oxa-Tf	Oxalate-transferrin, a chemical mutant modified to inhibit iron release
PFA	Paraformaldehyde
PBS	Phosphate buffered saline

ROI	Region of interest
SVD	singular value decomposition
Tf	Transferrin
TfR	Transferrin receptor

References

[1]. Sheftel AD, Mason AB, Ponka P, The long history of iron in the Universe and in health and disease, Biochim. Biophys. Acta Gen. Subj 1820 (2012) 161–187, 10.1016/j.bbagen.2011.08.002.

[2]. Luck AN, Mason AB, Transferrin-mediated cellular iron delivery, in: Current Topics in Membranes, 2012, pp. 3–35, 10.1016/B978-0-12-394390-3.00001-X.

[3]. Ko M, Quiñones-Hinojosa A, Rao R, Emerging links between endosomal pH and cancer, Canc. Metastasis Rev 39 (2020) 519–534, 10.1007/s10555-020-09870-1.

[4]. Lee SH, Griffiths JR, How and why are cancers acidic? Carbonic anhydrase ix and the homeostatic control of tumour extracellular ph, Cancers 12 (2020) 1–23, 10.3390/cancers12061616.

[5]. Liu Y, Zuo S, Li X, Fan J, Cao X, Yu X, Yang Q, Interaction between V-ATPase B2 and (pro) renin receptors in promoting the progression of renal tubulointerstitial fibrosis, Sci. Rep 6 (2016) 1–15, 10.1038/srep25035. [PubMed: 28442746]

[6]. Öörni K, Rajamäki K, Nguyen SD, Lähdesmäki K, Plihtari R, Lee-Rueckert M, Kovanen PT, Acidification of the intimal fluid: the perfect storm for atherogenesis, JLR (J. Lipid Res.) 56 (2015) 203–214, 10.1194/jlr.R050252.

[7]. Khoo TC, Tubbesing K, Rudkouskaya A, Rajoria S, Sharikova A, Barroso M, Khmaladze A, Quantitative label-free imaging of iron-bound transferrin in breast cancer cells and tumors, Redox Biology 36 (2020) 101617, 10.1016/j.redox.2020.101617. [PubMed: 32863219]

[8]. Halbrooks PJ, Mason AB, Adams TE, Briggs SK, Everse SJ, The oxalate effect on release of iron from human serum transferrin explained, J. Mol. Biol 339 (2004) 217–226, 10.1016/j.jmb.2004.03.049. [PubMed: 15123433]

[9]. Khmaladze A, Jasensky J, Price E, Zhang C, Boughton A, Han X, Seeley E, Liu X, Holl MMB, Chen Z, Hyperspectral imaging and characterization of live cells by broadband coherent anti-Stokes Raman scattering (CARS) microscopy with singular value decomposition (SVD) analysis, Appl. Spectrosc 68 (2014) 1116–1122, 10.1366/13-07183. [PubMed: 25198903]

[10]. Khmaladze A, Ganguly A, Kuo S, Raghavan M, Kainkaryam R, Cole JH, Izumi K, Marcelo CL, Feinberg SE, Morris MD, Tissue-Engineered constructs of human oral mucosa examined by Raman spectroscopy, Tissue Eng. C Methods 19 (2013) 299–306, 10.1089/ten.tec.2012.0287.

[11]. Khmaladze A, Ganguly A, Raghavan M, Kuo S, Cole JH, Marcelo CL, Feinberg SE, Izumi K, Morris MD, Raman spectroscopic analysis of human tissue engineered oral mucosa constructs (EVPOME) perturbed by physical and biochemical methods, in: Biomedical Vibrational Spectroscopy V: Advances in Research and Industry, 2012, 10.1117/12.908281.

[12]. Yu C, Gestl E, Eckert K, Allara D, Irudayaraj J, Characterization of human breast epithelial cells by confocal Raman microspectroscopy, Canc. Detect. Prev 30 (2006) 515–522, 10.1016/j.cdp.2006.10.007.

[13]. You S, Tu H, Zhao Y, Liu Y, Chaney EJ, Marjanovic M, Boppart SA, Raman spectroscopic analysis reveals abnormal fatty acid composition in tumor micro- and macroenvironments in human breast and rat mammary cancer, Sci. Rep 6 (2016) 1–10, 10.1038/srep32922. [PubMed: 28442746]

[14]. Surmacki J, Musial J, Kordek R, Abramczyk H, Raman imaging at biological interfaces: applications in breast cancer diagnosis, Mol. Canc 12 (2013) 1–12, 10.1186/1476-4598-12-48.

[15]. Jasensky J, Boughton AP, Khmaladze A, Ding J, Zhang C, Swain JE, Smith GW, Chen Z, Smith GD, Live-cell quantification and comparison of mammalian oocyte cytosolic lipid content between species, during development, and in relation to body composition using nonlinear

vibrational microscopy, Analyst 141 (2016) 4694–4706, 10.1039/C6AN00629A. [PubMed: 27272931]

[16]. D'Brant LY, Desta H, Khoo TC, Sharikova A.v., Mahajan SD, Khmaladze A, Methamphetamine-induced apoptosis in glial cells examined under marker-free imaging modalities, J. Biomed. Opt 24 (2019) 1, 10.1117/1.JBO.24.4.046503.

[17]. Sharikova A, Foraida ZI, Sfakis L, Peerzada L, Larsen M, Castracane J, Khmaladze A, Characterization of nanofibers for tissue engineering: chemical mapping by Confocal Raman microscopy, Spectrochim. Acta Mol. Biomol. Spectrosc 227 (2020) 117670, 10.1016/j.saa.2019.117670.

[18]. Szalontai B, Debreczeny M, Fintor K, Bagyinka C, SVD-clustering, a general image-analyzing method explained and demonstrated on model and Raman micro-spectroscopic maps, Sci. Rep 10 (2020) 4238, 10.1038/s41598-020-61206-9. [PubMed: 32144407]

[19]. Khan S, Ullah R, Javaid S, Shahzad S, Ali H, Bilal M, Saleem M, Ahmed M, Raman spectroscopy combined with principal component analysis for screening nasopharyngeal cancer in human blood sera, Appl. Spectrosc 71 (2017) 2497–2503, 10.1177/0003702817723928. [PubMed: 28714322]

[20]. Sfakis L, Sharikova A, Tuschel D, Costa FX, Larsen M, Khmaladze A, Castracane J, Core/shell nanofiber characterization by Raman scanning microscopy, Biomed. Opt Express 8 (2017) 1025, 10.1364/BOE.8.001025. [PubMed: 28271000]

[21]. Ong YH, Lim M, Liu Q, Comparison of principal component analysis and biochemical component analysis in Raman spectroscopy for the discrimination of apoptosis and necrosis in K562 leukemia cells: errata, Opt Express 20 (2012) 25041, 10.1364/oe.20.025041.

[22]. Cynthia U, Orumie O. Onyinyechi, Principal component analysis and its derivation from singular value decomposition, Int. J. Stat. Probab 8 (2019) 183, 10.5539/ijsp.v8n2p183.

[23]. Klema VC, Laub AJ, The singular value decomposition: its computation and some applications, IEEE Trans. Automat. Contr 25 (1980) 164–176, 10.1109/TAC.1980.1102314.

[24]. Byrne SL, Chasteen ND, Steere AN, Mason AB, The unique kinetics of iron release from transferrin: the role of receptor, lobe–lobe interactions, and salt at endosomal pH, J. Mol. Biol 396 (2010) 130–140, 10.1016/j.jmb.2009.11.023. [PubMed: 19917294]

[25]. Ashton L, Brewster VL, Correa E, Goodacre R, Detection of glycosylation and iron-binding protein modifications using Raman spectroscopy, Analyst 142 (2017) 808–814, 10.1039/C6AN02516A. [PubMed: 28174761]

[26]. Frank C, Rienitz O, Jährling R, Schiel D, Zakel S, Reference measurement procedures for the iron saturation in human transferrin based on IDMS and Raman scattering, Metall 4 (2012) 1239, 10.1039/c2mt20183f.

[27]. Abe K, Zhao L, Periasamy A, Intes X, Barroso M, Non-invasive in vivo imaging of near infrared-labeled transferrin in breast cancer cells and tumors using fluorescence lifetime FRET, PloS One 8 (2013), e80269, 10.1371/journal.pone.0080269. [PubMed: 24278268]

[28]. Talati R, Vanderpoel A, Eladdadi A, Anderson K, Abe K, Barroso M, Automated selection of regions of interest for intensity-based FRET analysis of transferrin endocytic trafficking in normal vs. cancer cells, Methods 66 (2014) 139–152, 10.1016/j.ymeth.2013.08.017. [PubMed: 23994873]

[29]. Movasaghi Z, Rehman S, Rehman IU, Raman spectroscopy of biological tissues, Appl. Spectrosc. Rev 42 (2007) 493–541, 10.1080/05704920701551530.

[30]. Swain RJ, Stevens MM, Raman microspectroscopy for non-invasive biochemical analysis of single cells, Biochem. Soc. Trans 35 (2007) 544–549, 10.1042/BST0350544. [PubMed: 17511648]

[31]. Surmacki JM, Woodhams BJ, Haslehurst A, Ponder BAJ, Bohndiek SE, Raman micro-spectroscopy for accurate identification of primary human bronchial epithelial cells, Sci. Rep 8 (2018) 1–11, 10.1038/s41598-018-30407-8. [PubMed: 29311619]

[32]. Bogliolo L, Murrone O, Piccinini M, Ariu F, Ledda S, Tilocca S, Albertini DF, Evaluation of the impact of vitrification on the actin cytoskeleton of in vitro matured ovine oocytes by means of Raman microspectroscopy, J. Assist. Reprod. Genet 32 (2015) 185–193, 10.1007/s10815-014-0389-7. [PubMed: 25399064]

[33]. Kopec M, Imiela A, Abramczyk H, Monitoring glycosylation metabolism in brain and breast cancer by Raman imaging, Sci. Rep 9 (2019) 166, 10.1038/s41598-018-36622-7. [PubMed: 30655566]

[34]. Zuniga W, Jones V, Anderson S, Echevarria A, Miller N, Stashko C, Schmolze D, Cha P, Kothari R, Fong Y, Storrie-Lombardi M, Raman spectroscopy for rapid evaluation of surgical margins during breast cancer lumpectomy, Sci. Rep 9 (2019) 14639, 10.1038/s41598-019-51112-0. [PubMed: 31601985]

[35]. Bi X, Rexer B, Arteaga CL, Guo M, Mahadevan-Jansen A, Evaluating HER2 amplification status and acquired drug resistance in breast cancer cells using Raman spectroscopy, J. Biomed. Opt 19 (2014), 025001, 10.1117/1.jbo.19.2.025001. [PubMed: 24496495]

[36]. Tubbesing K, Ward J, Abini-Agbomson R, Malhotra A, Rudkouskaya A, Warren J, Lamar J, Martino N, Adam AP, Barroso M, Complex Rab4-Mediated Regulation of Endosomal Size and EGFR Activation, Molecular Cancer Research, 2020, 10.1158/1541-7786.MCR-19-0052 molcanres.0052.2019.

[37]. Bogaerts J, Johannessen C, On/off resonance Raman optical activity of human serum transferrin, J. Raman Spectrosc 50 (2019) 641–646, 10.1002/jrs.5570.

[38]. Cao H, Chen J, Krueger EW, McNiven MA, SRC-mediated phosphorylation of dynamin and cortactin regulates the “constitutive” endocytosis of transferrin, Mol. Cell Biol 30 (2010) 781–792, 10.1128/MCB.00330-09. [PubMed: 19995918]

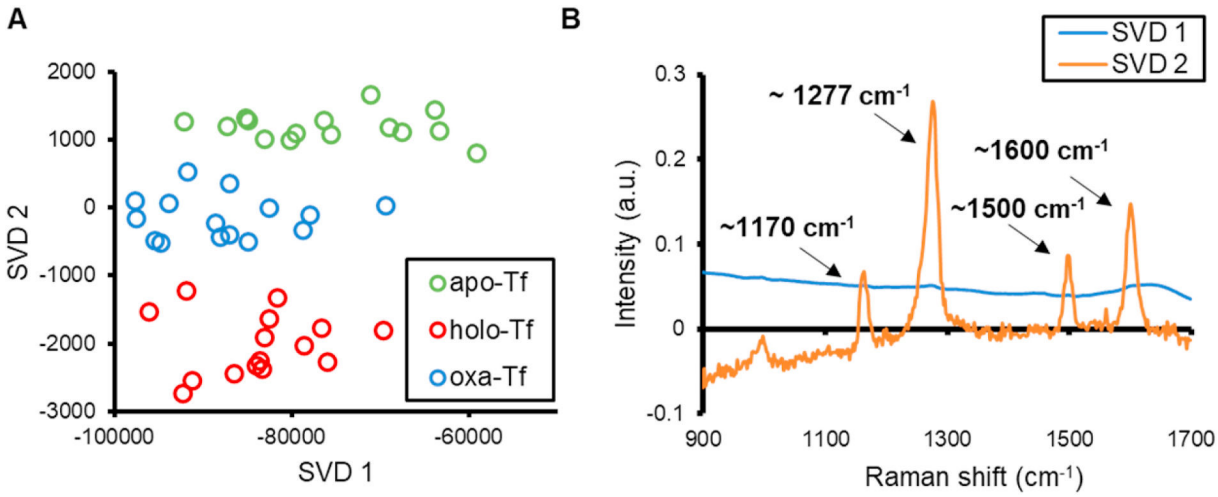

Fig. 1. SVD analysis provides a method of distinguishing apo-Tf, holo-Tf, and oxa-Tf proteins in solution.

Purified protein samples in solution (5 mg/mL in PBS) were subjected to the Raman imaging with a 20 × immersion objective, excitation at 532 nm, followed by the SVD analysis. (**A**) SVD scatter plot of the Raman spectra of apo-Tf, holo-Tf, and oxa-Tf. (**B**) Leading SVD components used to generate SVD scatter plot; dominant features are labeled with arrows. n = 15 spectra from a representative experiment. Representative spectra in Supplementary Fig. 1. Dehydrated samples of purified Tf were evaluated similarly and are provided in Supplementary Fig. 2.

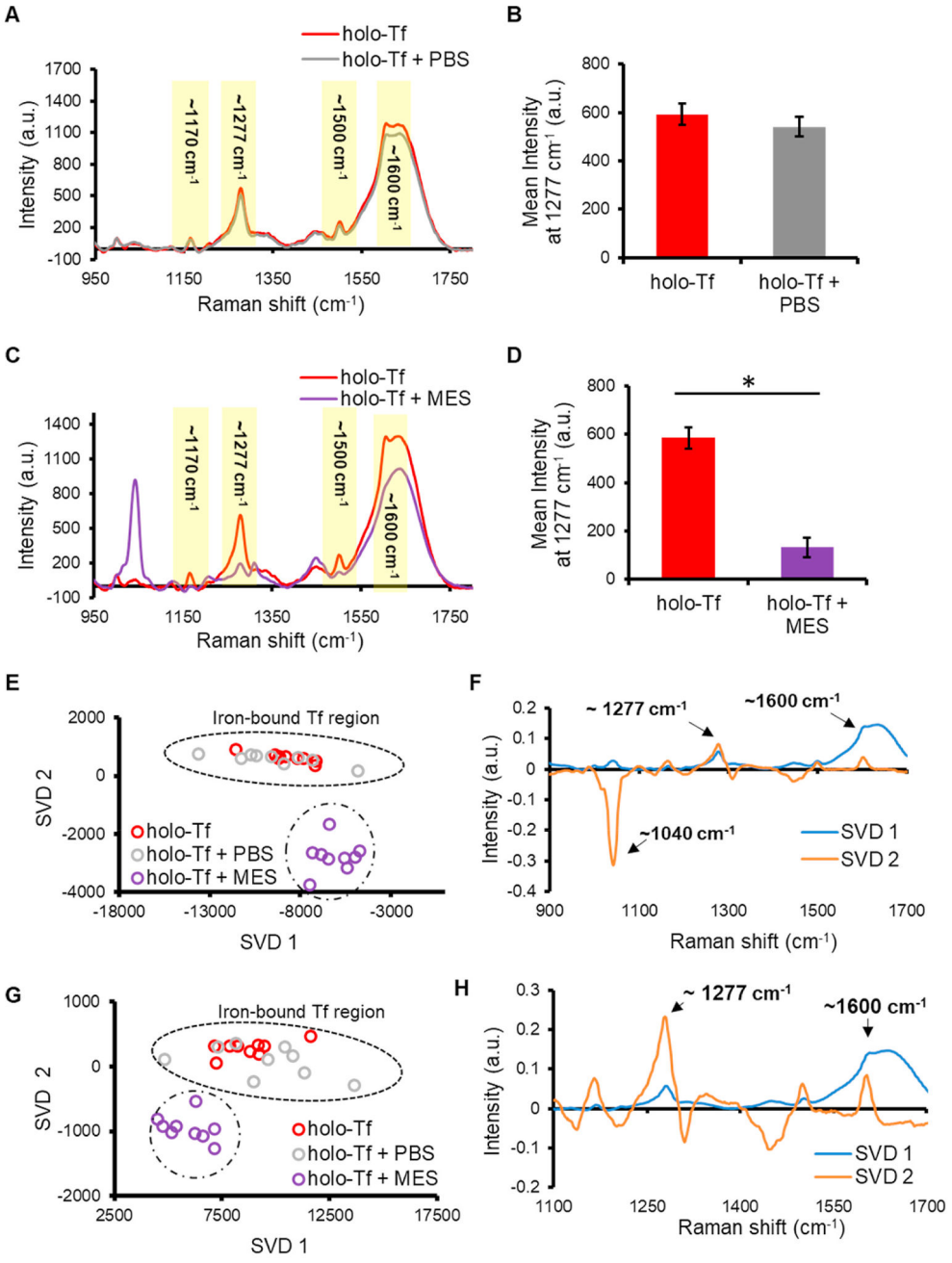

Fig. 2. Reduction of 1277 cm^{-1} Raman peak intensity indicates iron-release from Tf in-vitro.

Spectra of holo-Tf (5 mg/mL in PBS) before (red) and after the addition of either 100 mL neutral PBS (grey) or 100 mL iron-releasing MES buffer (purple). The focus for individual peak quantification is ~1277 cm^{-1} peak, which is drastically reduced upon the iron loss from Tf; other Tf associated peaks (1170, 1500, and 1600 cm^{-1}) are also reduced (highlighted in yellow). SVD analysis also provides separation of iron-bound Tf from iron-free Tf. (**A**) Representative Raman spectra of holo-Tf before (red) and after (grey) the addition of more neutral PBS. (**B**) Quantification of ~1277 cm^{-1} peak intensity of holo-Tf before (red) and after (grey) the addition of more neutral PBS. (**C**) Representative Raman spectra of holo-Tf

before (red) and after (purple) the addition of iron-releasing MES buffer. (**D**) Quantification of ~1277 cm^{-1} peak intensity of holo-Tf before (red) and after (purple) the addition of iron-releasing MES buffer. Error bars indicate 95% confidence intervals, n = 3 independent experiments. Asterisk represents statistical significance of *t*-test with $p < 0.05$ (specific p-value = 0.0003). Individual experiments, which highlight reproducibility, are provided in Supplementary Fig. 3. (**E**) SVD analysis of the holo-Tf populations before (red) and after addition of either neutral PBS (grey) or iron-releasing MES buffer (purple). (**F**) Leading components contributing to the separation of iron-bound Tf from iron-free Tf in the SVD plot of Fig. 2E. (**G**) Modified SVD analysis of the holo-Tf populations before (red) and after addition of either neutral PBS (grey) or iron-releasing MES buffer (purple). Here the spectral range below 1100 cm^{-1}, containing the Raman contribution of MES buffer, was removed. (**H**) Leading components contributing to the separation of iron-bound Tf from iron-free Tf in the SVD plot of Fig. 2G.

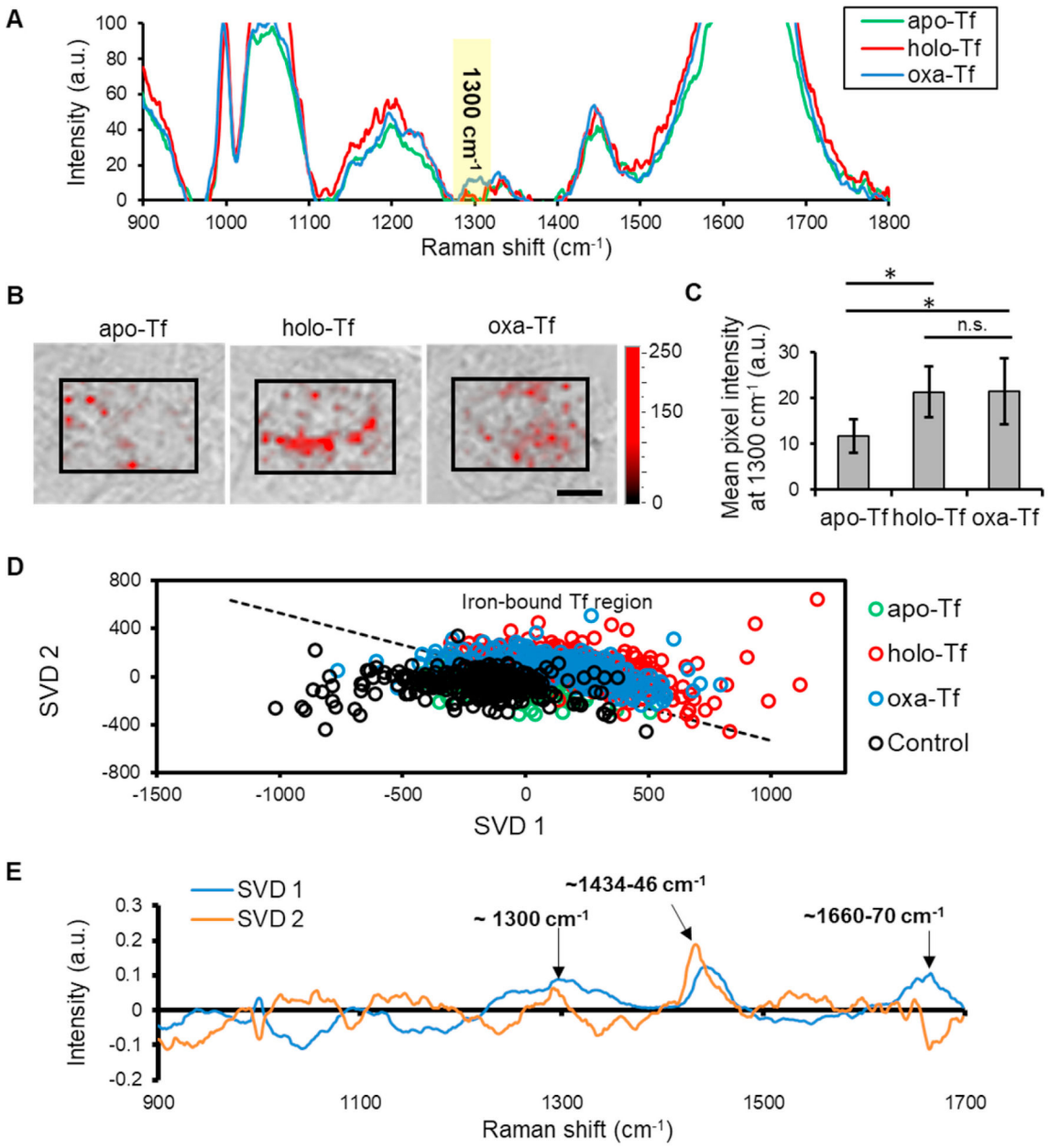

Fig. 3. Raman hyperspectral images and quantitative analysis of T47D breast cancer cells incubated with apo-Tf, holo-Tf, and oxa-Tf for 5 min show similarities between the iron-bound holo-Tf and oxa-Tf populations.

(**A**) Representative Raman spectra of T47D breast cancer cells incubated with apo-Tf, holo-Tf, and oxa-Tf for 5 min. (**B**) Subcellular mapping of the Raman 1300 cm^{-1} peak superimposed on the cell images, which are predominantly zoomed into the perinuclear region. *The intensity overlay is similar to the traditional endocytic (puncta) staining*. Scale bar = 10 μm. (**C**) Quantification of Raman 1300 cm^{-1} peak. Representative experiment, spectra normalized to ~1000 cm^{-1} phenylalanine peak, control cells average intensity at 1300 cm^{-1} used for background subtraction. n = 10 ROI per condition, error bars = 95% confidence interval, * indicates significance with $p < 0.05$ (specific p-values: apo-Tf vs.

holo-Tf p = 0.013, apo-Tf vs. oxa-Tf p = 0.038). (**D**) SVD scatter plot of Raman spectra for T47D cells incubated with apo-Tf, holo-Tf and oxa-Tf for 5 min. Spectra normalized to ~1000 cm^{-1} phenylalanine peak. Diagonal dotted line is used to separate populations for quantification (Fig. 5A). Individual populations shown in Supplementary Fig. 4. (**E**) The leading components SVD1 and SVD2 used to generate the scatter plot.

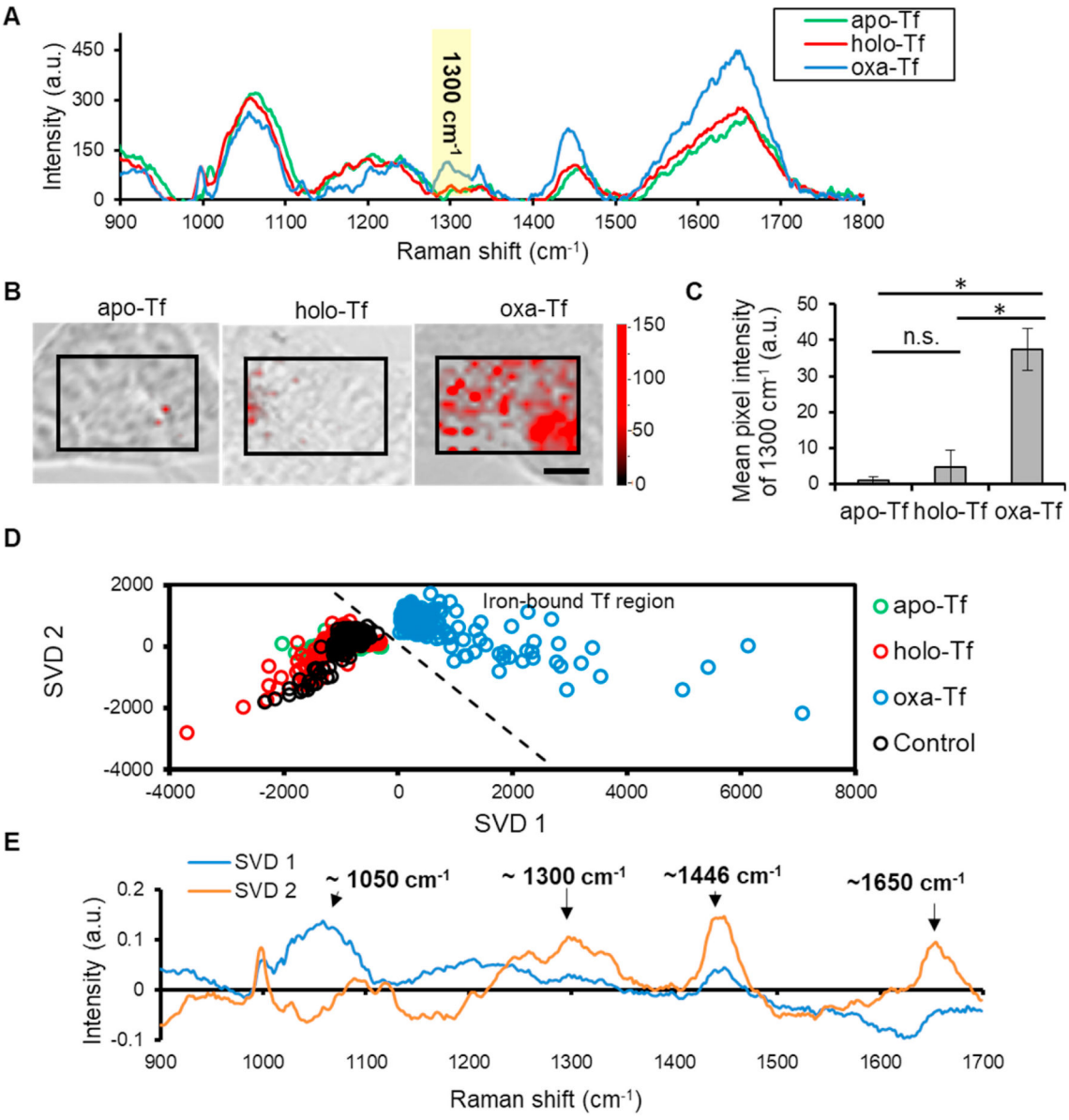

Fig. 4. Raman hyperspectral images and quantitative analysis of T47D incubated with apo-Tf, holo-Tf, and oxa-Tf for 5 min followed by a wash and 55 min iron-release chase.

(**A**) Representative Raman spectra. **(B)** Subcellular mapping of the Raman 1300 cm^{-1} peak superimposed on the cell images, which are predominantly zoomed into the perinuclear region. *The intensity overlay is similar to the traditional endocytic (puncta) staining*. Scale bar = 10 μm. (**C**) Quantification of Raman 1300 cm^{-1} peak. Representative experiment, spectra normalized to ~1000 cm^{-1} phenylalanine peak, control cells average intensity at 1300 cm^{-1} used for background subtraction. n = 10 ROI per condition, error bars = 95% confidence interval, * indicates significance with $p < 0.05$ (specific p-values: apo-Tf vs. oxa-Tf p = 1.0E-9, holo-Tf vs. oxa-Tf p = 1.5E-7). (**D**) SVD scatter plot of Raman spectra for T47D cells incubated with apo-Tf, holo-Tf and oxa-Tf for 5 min with 55 min chase. Spectra normalized to ~1000 cm^{-1} phenylalanine peak. Diagonal dotted line is used to separate populations for quantification (Fig. 5B). Individual populations shown in Supplementary

Fig. 5. (**E**) The leading components SVD1 and SVD2 used to generate the scatter plot, with significant peaks labeled.

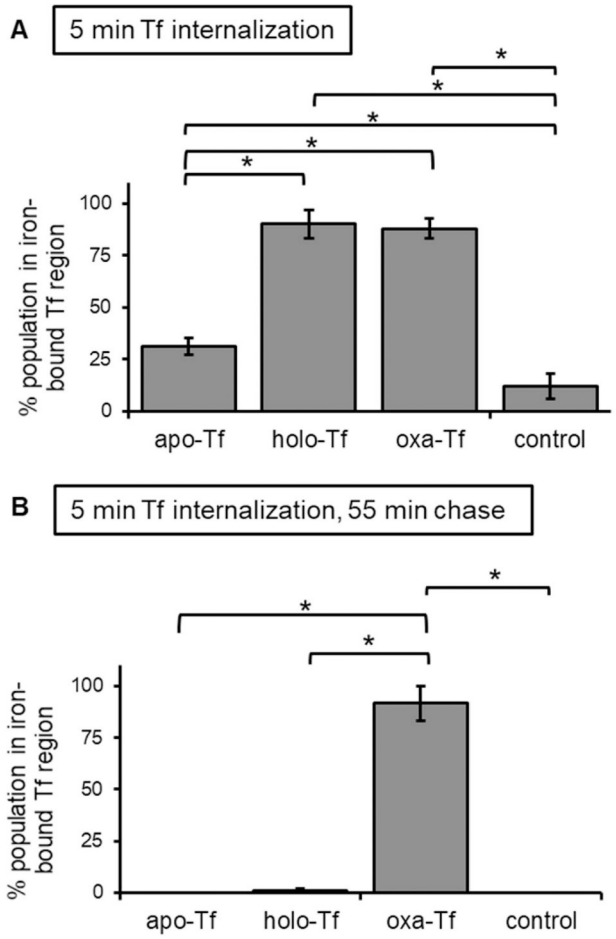

Fig. 5. Unloading of holo-Tf populations demonstrated with SVD analysis of Raman hyperspectral datasets.

The percent of spectral datapoints in SVD scatter plots which are clustered with oxa-Tf, and therefore located in the "iron-bound Tf region" of scatter plots were pooled from 3 independent experiments (**A**) 5 min Tf internalization percent distribution data from scatter plots in Fig. 3D and Supplementary Fig. 6A and 6C, three independent cell experiments, 180–300 spectra per experiment, * indicates statistical significance with p = 0.05 (Bonferroni correction for multiple comparisons) two-tailed *t*-test, left to right significant p-values = 0.0001, 6.25E-05, 0.0071, 7.91E-05, 4.89E-05. (**B**) 5 min Tf internalization followed by 55 min chase percent distribution data from scatter plots in Fig. 4D and Supplementary Fig. 7A and 7C, three independent cell experiments, 180–300 spectra per experiment, * indicates statistical significance with p = 0.05 (Bonferroni correction for multiple comparisons) two-tailed *t*-test, left to right significant p-values = 2.89E-05, 3.17E-05, 2.89E-05.